Nuclear and magnetic medium-range order in Tb_xSi_{1-x} amorphous alloys (x=0.59, 0.87) containing hydrogen

1992 J. Phys.: Condens. Matter 4 9697

(http://iopscience.iop.org/0953-8984/4/48/022)

J. Phys.: Condens. Matter 4 (1992) 9697–9708. Printed in the UK

Nuclear and magnetic medium-range order in Tb_xSi_{1-x} amorphous alloys ($x = 0.59, 0.87$) containing hydrogen

B Boucher and R Tourbot

Service de Physique de l'État Condensé†, CE de Saclay F-91191, Gif-sur-Yvette Cédex, France

Received 25 July 1992, in final form 10 August 1992

Abstract. Small-angle neutron scattering measurements were carried out on $(Tb_{0.59}Si_{0.41})H_{0.15}$ and $(Tb_{0.87}Si_{0.13})H_{0.15}$ amorphous alloys above and below the magnetic ordering temperature for zero field cooled (ZFC) and field cooled (FC) samples. From the measurements we have determined the spatial variation of the nuclear and magnetic scattering length per unit volume and describe the nuclear and magnetic medium-range order (MRO) for ZFC and FC samples. The existence of large nuclear and magnetic domains (or of nuclear and magnetic fluctuations) extending over a few hundred Angströms coexisting with less extended (a few tens of Angströms) fluctuations is shown. Moreover some small nuclear or magnetic inhomogeneities are found to exist and they seem to contain most of the 15 atomic per cent of hydrogen which have been detected in our sample composition. An applied magnetic field tends to align the local magnetization, but does not increase the spatial extension of fluctuations or domains, locked by the nuclear MRO, although their contrast is found to decrease. The comparison with the amorphous alloy $Tb_{65}Cu_{35}$ shows the generality of these results but does not allow us to understand the difference in the macroscopic magnetic properties, in particular the difference between the hysteresis loops.

1. Introduction

The amorphous alloys of magnetic rare earth (RE) and non-magnetic metals such as Cu, Ag and Al exhibit some magnetic properties which are easier to interpret than those of alloys of two magnetic ions. The nuclear or magnetic medium-range order (N-M-MRO) has been extensively studied for Cu or Al based alloys (Boucher and Chieux 1991) and is characterized by an intense scattering at low momentum transfer q, varying as q^{-N} or $L^{N/2}$ (L being a Lorentzian $1/(q^2+\kappa^2)$ and N an integer), and a much smaller scattering at high q values varying as a Guinier term. Thus small-angle neutron scattering (SANS) shows the existence of composition and/or magnetization fluctuations extending over a few hundred Angströms and of small aggregates ($\sim$ ten Angströms) carrying a specific magnetization, different in magnitude and direction from the bulk magnetization of the amorphous alloy. This magnetic configuration has been called 'seedy magnetic order' (Boucher *et al* 1986).

In order to show that these spectacular properties are general and can be found in numerous RE based amorphous alloys, we have studied the systems $(Tb_xSi_{1-x})H_{0.15}$ ($x = 0.59, 0.87$). The values chosen for x are larger than the percolation threshold

† Laboratoire de la Direction des Sciences de la Matière du Commissariat à l'Energie Atomique.

0953-8984/92/489697+12$07.50

and, for these values, silicon can be considered as metallic (Simonnin 1984, Simonnin *et al* 1986). The metallic silicon atomic size is of the order of the copper atom size (10.5 and 12 Å^3 respectively). Thus both Si alloys can be considered as roughly similar to $Tb_{65}Cu_{35}$ (Simonnin *et al* 1986, 1987, Boucher *et al* 1989a, 1991a, b). The results of neutron diffraction measurements are in agreement with this statement. They show coordination numbers between first neighbours that are not very different from those expected from a statistical atomic distribution. At high temperature ($T > 100$ K) the $(Tb_xSi_{1-x})H_{0.15}$ alloys are paramagnetic, obeying a Curie law. For $T < 57$ and 66 K for $x = 0.59$ and 0.87 respectively, the $(Tb_xSi_{1-x})H_{0.15}$ alloys show an asperomagnetic order with the same order of magnitude for their magnetization taken between first neighbours only or extended to a volume of radius 5 Å. However, the response to an applied field reveals significant differences, the viscous behaviour being much more important and the anisotropy much stronger for the Si than for the Cu alloys. At low temperature (4 K) 5 T are enough to saturate a hysteresis loop of copper terbium alloy and a $H^{-1/2}$ dependence is required to reach saturation (Boucher *et al* 1991a), while 15 T or more are necessary to saturate the hysteresis loop of Si alloys irrespective of the value of x (Simonnin *et al* 1986). It would be interesting to determine, if possible, the pertinent structural parameters that could explain more explicitly the magnetization response to an applied field. It is with this aim that we have studied N-M-MRO in these alloys by SANS. In this paper we report the experimental data and their processing; then we give an interpretation of our results.

2. Experimental details and data analysis

The samples were obtained by sputtering. The sheets were crushed into powder. They contained about 15 at.% of hydrogen (chemical analysis, neutron incoherent scattering analysis) (Simonnin *et al* 1986); the various measurements (magnetic measurements, neutron diffraction and SANS) were performed on the same samples. For the SANS measurements the powder was contained in a cylindrical cell with its axis parallel to the incident beam. The windows of the cell were in Suprasil glass giving no scattering at low q.

The SANS measurements were performed on the spectrometer PAXY at the laboratory Leon Brillouin† (LLB CE Saclay, France). The detection was achieved with a planar 64 × 64 cells detector allowing us to detect anisotropic scattering. A large q range was measured: $3.5 \times 10^{-3} < q = 4\pi \sin\theta/\lambda < 0.2$ Å^{-1}. The cell was located in a displex allowing us to vary the sample temperature between 10 and 300 K. A magnetic field (up to 0.65 T) was applied along a horizontal q scattering vector. It was possible to measure the sample scattering following field cooled (FC) or zero field cooled (ZFC) procedure. The measurements were scaled by comparison with a vanadium plate scattering. It was then possible to combine these results with those taken on 7 C (neutron diffraction spectrometer at LLB) at high and low temperature but without applied field. Therefore we were able to obtain the whole pattern for q up to 1 Å^{-1} (or more). On both spectrometers, the counting time was chosen to have a statistical accuracy of about 3‰.

The patterns taken at room temperature were corrected for cryostat, paramagnetism, hydrogen and background scattering to obtain the nuclear cross section.

† Laboratoire mixte CEA–CNRS.

Below the asperomagnetic ordering temperature, the magnetic scattering was directly obtained from the difference between low and room-temperature raw data (Boucher *et al* 1986)

To extract the variation of the scattering length per unit volume, b/v, from the experimental data and to reach the medium-range order (MRO) we needed to fit the patterns with analytical formulae, then to Fourier transform them. In a recent paper (Boucher and Chieux 1991) we discussed such a method, for example for the *a priori* choice between two formulae at the lowest q values: Lorentzian L to the power $N/2$ ($N = 2,3,4$) or q^{-N} law and we showed that it allowed us to reach the characteristic parameters (correlation length or size of a cluster, amplitude of variation of concentration or magnetization) which were not very different for the two formulae and seemed physically very reasonable. But it is necessary to remember that the choice of a formula implies the choice of a model; for example, a Lorentzian squared leads to a fluctuation of composition while a q^{-4} law can be interpreted as a juxtaposition of domains of different atomic concentration. In any case in this paper we fit the experimental curves at low q with Lorentzian to various powers, although no indication of a levelling-off of the scattering can be detected; at the lowest q values the correlation length ($\xi = 1/\kappa$) is determined from the slope of the curve in its steepest part, which is not a very precise method. In some cases, we can only indicate that κ is smaller than a given value.

For the high q values we have an identical problem; we choose to fit the data with e^{-cq^2} terms, which can be interpreted as a Guinier law or as a Fourier transform of another exponential, e.g. as non-interacting clusters imbedded in a matrix of different composition or as a sharp variation of the amplitude of the scattering length by unit volume over a small distance.

In spite of these difficulties we can be confident in the order of magnitude of the amplitude of variation of b/v and in its spatial extension. Indeed we have to note that the magnetic contrast involves two parameters: the amplitude and the direction of the magnetization. It follows that the contrast variation can be much sharper and stronger than in the nuclear case.

3. Experimental results

Figure 1 shows the traces through the experimental point of the q dependence of the nuclear (300 K) and the magnetic (13 K) ZFC and FC scattering on linear scale. We observe a sharp variation of the scattering at low q and a lesser one at high q values. The magnetic scattering shows a profile different from the nuclear scattering with an intense signal for $q \sim 0.03\,\text{Å}^{-1}$ which is reduced by an applied field.

3.1. Fits and numerical results

In order to fit measurements over such a large range of q measurements, it is necessary to take a scattering law composed of several terms, each of them being best adapted to a defined and restricted range of q. The lack of data at very low q values ($q < 2.10^{-3}$ Å^{-1}) renders difficult the choice of the low q term of the scattering equation. This explains why several combinations of the terms composing the scattering equation had to be used to satisfactorily describe our data, e.g.

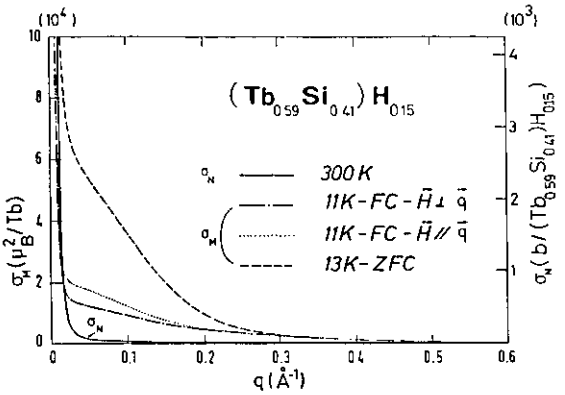

Figure 1. Variation of the nuclear and magnetic cross sections σ_N in barns per $(Tb_{0.59}Si_{0.41})H_{0.15}$ and σ_M in $\mu_B^2 Tb^{-1}$ against $q(Å^{-1})$ as obtained for ZFC and FC samples. We observe an important magnetic scattering, very sensitive to the applied field action.

$$\sigma = 4\pi\frac{d\sigma}{d\omega} = \frac{A_4}{(q^2+\kappa_4^2)^2} + \frac{A_2}{(q^2+\kappa_2^2)} + B_1\,e^{-c_1q^2} + B_2\,e^{-c_2q^2} \tag{1}$$

or

$$\sigma = 4\pi\frac{d\sigma}{d\omega} = \frac{A_3}{(q^2+\kappa_3^2)^{3/2}} + \frac{A_2}{(q^2+\kappa_2^2)} + B_1\,e^{-c_1q^2} + B_2\,e^{-c_2q^2}. \tag{2}$$

Under these conditions, a 'goodness of fit' criterion allowed us to optimize the term of the scattering law which dominates in each restricted q range, but difficulties are encountered with its contributions to the neighbouring ranges which obliges us to correct the parameters. For a chosen relation (1 or 2), the agreement between calculated and experimental data can be obtained for a set of parameters, each in a range of values. Outside this range, the caluclated curve deviates substantially from the experimental one. These ranges give an idea of the accuracy of the parameters.

We tried to use self-constant fitting procedures for data accumulated over such a large scale of momentum transfer, with differences in statistical accuracy which can vary considerably between different parts of the scale, depending on the conditions of data acquisition (e.g. sample to detector distance). For example, a trial to fit out general equation (1) to the most extensive set of data ($TB_{87}Si_{13}$ at 13 K) does not converege unless we simplify the equation (e.g. by dropping the L term). This will not greatly affect the physical quantities since the first Gaussian term will then replace the L term with a radius of gyration of 26 Å in good agreement with the correlation length of 29 Å previously obtained from L. Nevertheless, the simplified equation does not give results in agreement with experimental data for the whole scale, and particularly cannot reproduce well the slow drop obtained at high q values. Therefore it is very difficult to use any global criterion to describe quantitatively the quality of the fit. Comparison of the experimental and theoretical curves remains the best procedure to allow us to judge the agreement achieved in the various parts of the spectrum. The selection of our master equation based on detailed analysis of the various sections of the curve is considered as a safe basis for the data description.

The first two terms of equations (1) and (2) (written as L^2 and L or $L^{3/2}$ and L) can be fitted almost independently over distinct q ranges as discussed in Boucher

and Chieux (1991); the A_i parameters are obtained with a accuracy of ±7%. The κ_3 value of the $L^{3/2}$ term is very small, its upper limiting value being 10^{-3}Å^{-1} while κ_4 and κ_2 are known with an accuracy of only ±40%. The exponential terms are more difficult to be fitted and the uncertainty in B_i and c_i is of the order of 50%. Following Teixeira (1992) these terms, which represent the effect of discrete inhomogeneities, can be used for values of qr as large as one or more. In the present case these inhomogeneities can only be semi-quantitatively described.

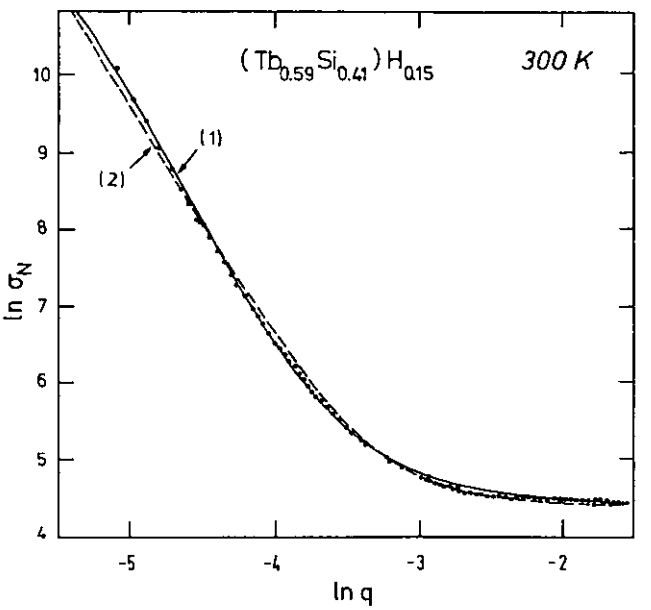

Figure 2. Ln–ln representation of fits for σ_N(300 K) of $(Tb_{0.59}Si_{0.41})$ $H_{0.15}$; points: experimental; full and broken curves: calculated, following relation (1) or (2).

The agreement obtained between the scattering relations (1) and (2) and the data is displayed in figure 2. Measurements at lower q values that would help in the determination of the low q scattering law are being considered. Values of fitted parameters are reported in table 1. Table 2 gives the expressions for the contrast $K(r)$ deduced by the Fourier transform (FT) of the scattering formulae. The contrast is the difference between the scattering length per unit volume taken at two points 1 and 2 a distance apart r, $K(r) = (b_1/v_1 - b_2/v_2)$. It varies as an amplitude D_i or E_i multiplied by a function of r containing the constants $\kappa_i = 1/\xi_i$ and c_i. From c_i we deduce a spherical particle size characterized by its radius that we call ξ_i'; ξ_i is a correlation length that characterizes the spatial extension of the fluctuations. Table 3 gives the values of different parameters which describe the MRO in real space. The D_i parameters related to the $L^{N/2}$ terms are known with good accuracy (±4%). The parameters E_i related to the exponential terms are less accurately known (±25%) and need some comments. In the case when the exponential terms are due to discrete inhomogeneities, the B_i factors in relation (1) or (2) have to be multiplied by φ^{-1}, where φ is the volume function occupied by the inhomogeneities. The real contrast is then the apparent contrast E_i (table 3) increased by a factor $\varphi^{-1/2}$. Although in a favourable case, for $(Tb_{0.59}Si_{0.41})H_{0.15}$, Simonnin (1984) was able to determine φ ($0.05 < \varphi < 0.1$), the signal-to-noise ratio of the SANS data was generally too low to obtain it.

Table 1. Parameter values obtained by fitting of the experimental cross sections with relation (1) or (2). The nuclear cross section is expressed in barns per formula unit of $(Tb_xSi_{1-x})H_{0.15}$ and the magnetic cross section in square Bohr magnetons per Tb atom; κ_i is in $Å^{-1}$ and c_i in $Å^2$; the other parameters are defined accordingly.

$(Tb_{.59}Si_{.41})H_{.15}$		A_4	κ_4	A_2	κ_2	A_3	κ_3	A_2	κ_2	B_1	c_1	B_2	c_2
σ_N 300 K	b/$Tb_{.59}Si_{.41}$	5.0×10^{-5}	3.2×10^{-3}	7.5×10^{-2}	3.2×10^{-3}					17.0	2.8	8.6	15.0
						4.3×10^{-3}	$<10^{-3}$	0	0	20.0	3.0	3.0	15.0
σ_M 13 K ZFC	$\mu_B^2Tb^{-1}$	3.0×10^{-4}	5.0×10^{-3}	7	5.0×10^{-3}					5.2×10^4	50.0	5.6×10^3	8.4
						8.0×10^{-3}	10^{-2}	7	5.0×10^{-4}	5.2×10^4	50.0	5.6×10^3	8.4
11 K FC													
$q \parallel H$		3.4×10^{-4}	5.0×10^{-3}	1	5.0×10^{-2}					1.4×10^4	70.0	5.9×10^3	8.4
						2.0×10^{-2}	$<10^{-3}$	0	0	1.4×10^4	70.0	5.9×10^3	8.4
$q \perp H$		5.0×10^{-4}	5.0×10^{-3}	1	5.0×10^{-2}					7.5×10^3	70.0	5.9×10^3	8.4
						3.0×10^{-2}	$<10^{-3}$	0	0	7.5×10^3	70.0	5.9×10^3	8.4

$(Tb_{.87}Si_{.13})H_{.15}$		A_4	κ_4	A_2	κ_2	A_3	κ_3	A_2	κ_2	B_1	c_1	B_2	c_2
σ_N 300 K	b/$Tb_{.87}Si_{.13}$	7.0×10^{-5}	3.0×10^{-3}	0.126	3.0×10^{-3}					89	50.0	20.0	1.4
						6.4×10^{-3}	$<10^{-3}$	0	0	101	50.0	20.5	1.4
σ_M 13 K ZFC	$\mu_B^2Tb^{-1}$	2.0×10^{-5}	3.0×10^{-3}	14	3.5×10^{-2}					0	0	2.0×10^3	3.8
						2.0×10^{-3}	$<10^{-3}$	13.4	3.5×10^{-2}	0	0	2.0×10^3	3.8

Table 2. Scattering laws and corresponding contrast. The cross section for isotropic scattering σ is defined in barns per formula unit or $\mu_B^2 Tb^{-1}$. The average volume occupied by a formula unit is v. The contrast $K(r) = (b_1/v_1 - b_2/v_2)$ is the difference between the scattering length per unit volume for two volumes, v_1 and v_2, at a distance r from each other. The contrast $K(r)$ is expressed in 10^{-12} cm Å^3, or μ_B Å^{-3}; A, κ, B and c are constants, $K_0(\kappa r)$ is a modified Bessel function.

σ	$K(r)$
$A/(q^2+\kappa^2)^2$	$(A/32\pi^2 v\kappa)^{1/2}\,e^{-\kappa r/2}$
$A/(q^2+\kappa^2)^{3/2}$	$(A/8\pi^3 v)^{1/2}\left(K_0(\kappa r)\right)^{1/2}$
$A/(q^2+\kappa^2)$	$(A/16\pi^2 v)^{1/2} r^{-1/2}\,e^{-\kappa r/2}$
$B\,e^{-cq^2}$	$(B/32\pi^{5/2} v c^{3/2})^{1/2}\,e^{-r^2/8c}$

3.2. Applied-field influence

With a bidimensional detector it is possible to measure the scattering in well defined directions and particularly for a transfer vector q parallel to the applied horizontal field H and for q perpendicular to H. In the first case the scattering is proportional to the magnetization component along the vertical direction, and in the second case it is proportional to the component parallel to H.

The magnetic correlation length corresponding to terms L^2 (and perhaps $L^{3/2}$) is the same for the FC and the ZFC sample, and has a value near the nuclear correlation length, indicating a relation between nuclear and magnetic order. The contrast coefficients D_4 or D_3 increase slightly with the applied field. On the other hand, the magnetic order corresponding to L scattering is reduced to a much smaller extension (20 Å instead of 200 Å) and the contrast coefficient D_2 is reduced by about a factor three.

The scattering due to inhomogeneities (exponential terms) decreases with the applied field.

4. Interpretation and discussion

Our SANS results have been attributed to the bulk and not to the surface of the samples for several reasons. (i) $Tb_{65}Cu_{35}$ tape or powder give similar patterns. (ii) Measurements on $Tb_{65}Cu_{35}$ tape immersed in methanol (the contrast variation method) showed that the scattering was due to the bulk, the surface participating for less than 5%. (iii) The order of magnitude of the scattering on an absolute scale suggests that it would be very difficult to account for it by surface effects (Boucher *et al* 1989b).

4.1. The presence of hydrogen

Both alloys have a non-negligible hydrogen content, of the order of 1.6 times that present in sputtered $Tb_{65}Cu_{35}$. For $(Tb_{0.59}Si_{0.41})H_{0.15}$ Simonnin (1984) has shown the existence of aggregates of SiH_y ($y \sim 3,4$) of radius 4 Å and occupying 5% of the sample volume. But it is also possible to find hydrogen as interstitial atoms in the amorphous $(Tb_xSi_{1-x})H_{0.15}$ alloy. For $Tb_{65}Cu_{35}$, we know that the sputtered samples containing hydrogen show nuclear and magnetic order less pronounced than the quenched sample without hydrogen (Boucher *et al* 1989a). It seems to be a general

Table 3. Parameters giving the contrast. D_i and E_i are the prefactors of the r functions giving $K(r)$ (table 2). D_i is relative to the FT of $L^{N/2}(N = i)$ and E_i relative to the FT of the exponential term. We have indicated in brackets the values of D_i and E_i parameters in $\mu_B Tb^{-1}$ to make easier the comparison with the full moment ($9\mu_B$). ξ_4, ξ_2, ξ_3, ξ_1' and ξ_2' are measured in Å.

$(Tb_{.59}Si_{.41})H_{.15}$		D_4	ξ_4	D_2	ξ_2	D_3	ξ_3	D_2	ξ_2	E_1	ξ_1'	E_2	ξ_2'
300 K	10^{-12} cm Å^{-3}	1.32×10^{-3}	310	4.50×10^{-3}	310					3.4×10^{-3}	11	1.7×10^{-2}	4.9
						8.60×10^{-4}	$> 10^3$	0	0	2.0×10^{-3}	11	1.7×10^{-2}	4.9
13 K ZFC	μ_BÅ^{-3}	2.20×10^{-3}	200	3.40×10^{-2}	200								
	$\mu_B Tb^{-1}$	(0.086)		(1.3)						8.2×10^{-2}	20	1.0×10^{-1}	8.2
						9.00×10^{-4}	$> 10^3$	3.36×10^{-2}	0	(3.21)		(4.0)	
						(0.035)		(1.30)					
11 K FC													
$q \parallel H$ $M \perp H$	μ_BÅ^{-3}	2.34×10^{-3}	200	1.27×10^{-2}	20								
$q \parallel H$ $M \perp H$	$\mu_B Tb^{-1}$	(0.092)		(0.5)						3.3×10^{-2}	24	1.0×10^{-1}	8.2
						1.43×10^{-3}	$> 10^3$	0	0	(1.28)		(4.0)	
						(0.056)							
$q \perp H$ $M \parallel H$	μ_BÅ^{-3}	2.84×10^{-3}	200	1.27×10^{-2}	20								
$q \parallel H$ $M \perp H$	$\mu_B Tb^{-1}$	(0.112)		(0.5)						2.4×10^{-2}	24	1.0×10^{-1}	8.2
						1.75×10^{-3}	$> 10^3$	0	0	(0.95)		(4.0)	
						(0.070)							

$(Tb_{.87}Si_{.13})H_{.15}$		D_4	ξ_4	D_2	ξ_2	D_3	ξ_3	D_2	ξ_2	E_1	ξ_1'	E_2	ξ_2'
300 K	10^{-12} cm Å^{-3}	1.50×10^{-3}	330	5.20×10^{-3}	330					3.9×10^{-3}	20	2.7×10^{-2}	3.3
						9.30×10^{-4}	> 330	0	0	4.2×10^{-3}	20	2.8×10^{-2}	3.3
13 K ZFC	μ_B Å^{-3}	8.00×10^{-4}	330	5.10×10^{-2}	29								
	$\mu_B Tb^{-1}$	(0.026)		(1.7)						0	0	1.2×10^{-1}	5.5
						4.90×10^{-4}	> 330	5.00×10^{-2}	29			(4.8)	
						(0.016)		(1.7)					

Table 4. Values of the contrast $K(r) = (b_\alpha/v_\alpha - b_\beta/v_\beta)$ for various impurities. The index α refers to the bulk $(Tb_xSi_{1-x})H_{0.15}$ and the index β to the impurity. The most probable impurities have been listed.

	$K(r) = (b_\alpha/v_\alpha - b_\beta/v_\beta)$ $(10^{-12}$ cm Å$^{-3})$	
Matrix ⟶	$Tb_{.59}Si_{.41}$	$Tb_{.87}Si_{.13}$
Impurity ↓		
Ar	0.0165	0.0142
Vacuum	0.0261	0.0238
Tb	0.0031	0.0008
Si	0.0054	0.0031
Tb_2O_3	−0.0151	−0.0174
TbH_2	0.0264	0.0241
TbH_3	0.0358	0.0335
TbSi	−0.0010	−0.0033
Tb_5Si_3	−0.0003	−0.0020
$TbSi_2$	−0.0031	−0.0055
SiH	0.0259	0.0218
SiH_2	0.0406	0.0383
SiH_3	0.0544	0.0521
SiH_4	0.0662	0.0638

trend in these alloys that hydrogen diminishes the magnetic ordering temperature and disperses the values of magnetic exchange interactions. However, it is not possible for us to describe in detail the role played by hydrogen.

4.2. Nuclear scattering

4.2.1. Low q values. For both alloys the nuclear scattering can be fitted either by relation (1) or relation (2) in which $A_2 = 0$. The maximum amplitudes corresponding to the values of A_4 or A_2 in relation (1) are of the same order whatever the value of x, and can be interpreted as fluctuations due to a Tb/Si composition variation of order $\Delta x \sim \pm 0.07$, e.g. between $Tb_{0.52}Si_{0.48}$ and $Tb_{0.66}Si_{0.34}$ for the first alloy, and $Tb_{0.79}Si_{0.21}$ and $Tb_{0.95}Si_{0.05}$ for the second (figure 3). This variation of composition could be strongly reduced by taking into account the hydrogen content. The correlation length is of the order of 300 Å.

The coexistence of the L^2 and L terms indicates the superposition of a sharply attenuated local fluctuation, $(D_2 r^{-1/2} e^{-\kappa r/2})$, on a more extended fluctuation $D_4 e^{-\kappa r/2}$. The question arises as to whether the origins of r appearing in the two terms are correlated or independent. Depending on this, the contrast would show interference effects or not. We are not able to decide on this question.

With the application of equation (2) the sum $(L^2 + L)$ is replaced by an $L^{3/2}$ term, whose FT $K_0(\kappa r)$ is a modified Bessel function with a smaller amplitude, i.e. a weaker variation of composition, but a correlation length larger than that of L^2. In the absence of measurements at very low q, we can only give a lower estimate for ξ, for both alloys $\xi > 10^3$ Å.

Figure 4 shows the different functions $K_i(r)$; the sum of $K_4(r) + K_2(r)$ is not very different from $K_3(r)$. In both cases the composition varies sharply inside a distance of about 20 Å and then slowly over a few hundred Angströms.

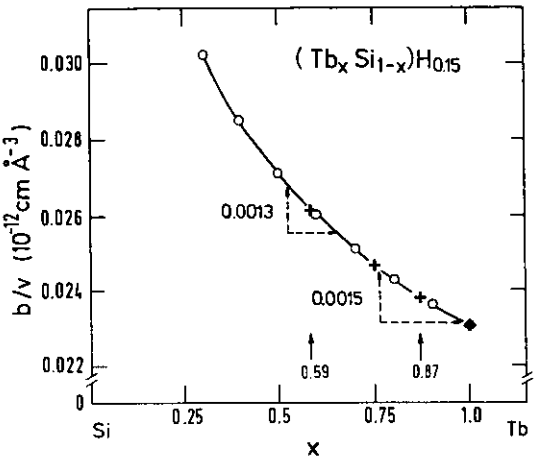

Figure 3. Variation of the nuclear scattering length per unit volume as a function of the concentration x in $(Tb_xSi_{1-x})H_{0.15}$.

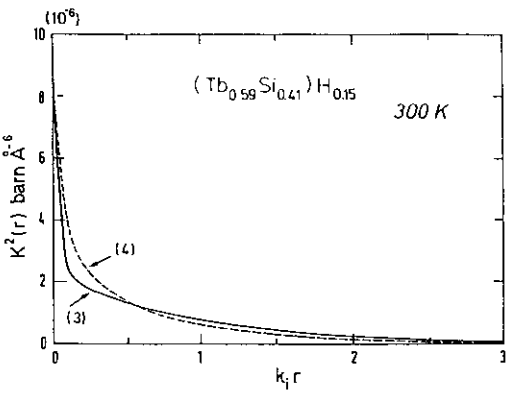

Figure 4. $(Tb_{0.59}Si_{0.41})H_{0.15}$ at 300 K. Squared nuclear contrast $K^2(r) = (D_4^2 + D_3^2 1/r)e^{-\kappa_4 r}(3)$ (full curve) and $K^2(r) = \gamma D_3^2\ K_0(\kappa_3 r)(4)$ (broken curve) calculated with the experimental parameters (tables 1 and 3); γ is a scaling coefficient ~ 2; K_0 is a modified Bessel function.

4.2.2. High q values. The intensity is much weaker than for low q scattering and extends to very high q values indicating the presence of discrete and small inhomogeneities.

We observe two kinds of exponential terms $B_i e^{-c_i q^2}$, of which one is with a strong apparent contrast $(E_2 \approx 2 \times 10^{-2}(10^{-12}\,\text{cm Å}^{-3}))$ and with a weak extension $(\xi_1' \sim 5$ Å) and is due to SiH_y. No other explanation was found to account for the high contrast and the low volume fraction ($\sim 5\%$) as shown by Simonnin (1984).

The other type of scattering corresponds to a wider spatial extension (~ 20 Å) and shows an apparent contrast which leads to a high variation of concentration unless hydrogen plays a role. It is not possible to give a detailed model; we can only reasonably suggest that this scattering is due to little clusters or inhomogeneities, distributed more or less at random and not strongly interacting with each other. This exponential scattering is thus very different from the L scattering, which indicates a sharp variation of contrast over about 20 Å, but extending over few hundred Angströms.

4.3. Magnetic scattering

4.3.1. Low q values. From the scattering at low q we obtain the contrast variation and, in particular, the maximum amplitude of the contrast, e.g. the difference between

the local magnetization and the magnetization of its surroundings, the latter being located at a distance $r \sim 2\pi/q \geqslant 2\pi\xi$. Note that two parameters occur for the magnetic contrast: the magnitude and the direction of the magnetization. When r is large we can think that the magnetization of the surroundings present a zero, or a very small average value, and the contrast can be approximated by the local magnetization at the centre. But this is not proven, because the ξ distance can be embedded within a larger magnetic domain not detectable with the present q range and whose magnetization is relatively high.

As already mentioned in several papers (Boucher *et al* 1986, 1990, Boucher and Chieux 1991) the magnetic scattering can be fitted by the same relations (1) or (2) as used for nuclear scattering, indicating the strong influence of the nuclear order on the magnetic order. Whatever the relation chosen, this scattering shows the existence of large domains (200–1000 Å or more) in which the magnetic contrast varies slightly (0.03–0.1 $\mu_B Tb^{-1}$). On these variations are superimposed magnetization variations, which are fairly extended ($\xi \sim 200$ Å), and very intense ($\sim 1.5\ \mu_B Tb^{-1}$) over only a few tens of Angströms (attenuated by an $r^{-1/2}$ factor). These magnetization variations give the L scattering. They can be compared to the full moment $9\mu_B Tb^{-1}$. When a field is applied (FC sample) the magnetization of the large domains is increased along the field by at least 40%, but the size of the domains is not changed and stays the same as the nuclear domain size. On the contrary, the intensity of the magnetization peaks and their spatial extension are reduced by a factor 2–3 for the magnetization and by a factor 10 for the extension. If relation (2) is used for the fit, the L term disappears when the field is applied. The field tends to diminish the contrast between the various parts of the sample by aligning the magnetization of the peaks and of the domains along its direction.

4.4. High q values

The nuclear scattering showed two kinds of inhomogeneities, one of which could be identified as non-magnetic (SiH_y). At low temperature the matrix magnetization creates with these 'holes' a contrast of a few Bohr magnetons ($\sim 4\mu_B$) per Tb atom, insensitive to an applied field. It indicates that the average magnetization around the 'holes' is high. Besides this type of contrast we observe, for $x = 0.59$, inhomogeneities of about 20 Å showing a high magnetic contrast and decreasing sharply with an applied field. These inhomogeneities are discrete and have to be distinguished from fluctuations which give rise to an L scattering (subsection 3.1.).

5. Conclusion

In the TbSi amorphous alloys containing hydrogen there exists a nuclear order over long distances (> 300 Å) corresponding to concentration fluctuations. We can also speak about 'domains' with composition variation near the domain border. In both cases the contrast can be reinforced by a characteristic distribution of hydrogen. We are not in a position to choose between the two descriptions. This nuclear order introduces a magnetic order spread over the same distance, but the corresponding variation of magnetization is weak $\simeq 0,1\,\mu_B Tb^{-1}$. Superimposed on these fluctuations, there exist some nuclear and magnetic fluctuations whose amplitudes are strong (a few 10^{-3} 10^{-12} cm Å^{-3} or a few Bohr magnetons per Tb)

but only over a few tens of Angströms. Such a high variation of the magnetization is due to a pronounced asperomagnetic order. Therefore the magnetic order is the superposition of two kinds of variations on two different scales. This self-similar behaviour could be investigated in more detail.

This study also shows the existence of discrete magnetic or non-magnetic inhomogeneities. The non-magnetic aggregates can be used as probes to measure the average magnetization around them, which is about $4\,\mu_B Tb^{-1}$.

The influence of an applied field during cooling tends to erase the fluctuations, increasing the magnetization along the field, but the large correlation lengths do not change indicating very clearly the importance of long-range nuclear order.

The comparison between TbCu and TbSi amorphous alloys containing hydrogen show that the MRO is similar and can be interpreted in the same way by fluctuations over distances of tens and hundreds Angströms and by the presence of local inhomogeneities, some of which are non-magnetic. Neutron diffraction (Boucher *et al* 1991b) shows that the short-range order of both alloys is also similar. It seems therefore that the differences observed in the macroscopic properties such as the hysteresis loops should be attributed to the electronic structures.

Acknowledgments

We are grateful to Dr P Chieux (Institut Laue Langevin, Grenoble, France) and J P Damay (HEI Laboratoire, Chimie Physique, CNRS-Lille) for very helpful discussions. We gratefully acknowledge Dr A Brulet and F Gibert, (Laboratoire Léon Brillouin, CE Saclay, France) for their help during the measurements.

References

Boucher B and Chieux P 1991 *J. Phys.: Cond. Matter* **3** 2207-29
Boucher B, Chieux P, Convert P, Tourbot R and Tournarie P 1986 *J. Phys. F: Met. Phys.* **16** 1821–43
Boucher B, Chieux P, Sanquer M and Tourbot R 1990 *J. Non Cryst. Sol.* **117/118** 191–4
Boucher B, El Gadi M, Sanquer M, Tourbot R and Bellissent R 1989a *J. Phys.: Condens. Matter* **1** 2057–66
Boucher B, Sanquer M, Tourbot R and Bellissent R 1991a *J. Phys.: Condens. Matter* **3** 1985–94
Boucher B, Sanquer M, Tourbot R, Chieux P and Maret M 1989b *J. Phys.: Condens. Matter* **1** 2647
Boucher B, Tourbot R and Bellissent R 1991b *J. Phys.: Condens. Matter* **3** 2843–8
Simonnin P 1984 *Thèse Univ. Paris 6, France*
Simonnin P, Tourbot R, Boucher B and Bellissent R 1987 *J. Phys. F: Met. Phys.* **17** 559–67
Simonnin P, Tourbot R, Boucher B, Perrin M and Vanhaute J 1986 *Phys. Stat. Sol (a)* **98** 551
Teixeira J 1992 *Structure and Dynamics of Supramolecular Aggregates and Strongly Interacting Colloids* ed. S H Chen, J S Huang and P Tartaglia (Dordrecht: Kluwer)